Electronic Supplementary Material (ESI) for Journal of Materials Chemistry A.

Electronic Supplementary Information

Lead-Free Low-Dimensional Tin Halide Perovskites with Functional Organic Spacers: Breaking the Charge-Transport Bottleneck

Ming-Gang Ju,[a] Jun Dai,[a] Liang Ma,[b] Yuanyuan Zhou,[c] Wanzhen Liang,[d] Xiao Cheng Zeng[a,e,*]

[a]Department of Chemistry, University of Nebraska-Lincoln, Lincoln, Nebraska, 68588, United States

[b]Southeast University, Nanjing 211189, China

[c]School of Engineering, Brown University, Providence, Rhode Island 02912, United States

[d]State Key Laboratory of Physical Chemistry of Solid Surfaces, Collaborative Innovation Center of Chemistry for Energy Materials, Fujian Provincial Key Laboratory of Theoretical and Computational Chemistry, and Department of Chemistry, College of Chemistry and Chemical Engineering, Xiamen University, Xiamen, Fujian 361005, China

[e]Department of Chemical & Biomolecular Engineering and Department of Mechanical & Materials Engineering, University of Nebraska-Lincoln, Lincoln, Nebraska, 68588, United States

Computational Methods

Density functional theory calculation. The first-principles computations for all periodic systems are performed based on density-functional theory (DFT) methods as implemented in the Vienna ab initio simulation package (VASP 5.4).[1] An energy cutoff of 520 eV is employed, and the atomic positions are optimized using Perdew-Burke-Ernzerhof (PBE) functional without any symmetric restrictions until the maximum force on each atom is less than 0.03 eVÅ^{-1}. The ion cores are described by using the projector augmented wave (PAW) method.[2] Grimme's DFT-D3 correction is adopted to describe weak van der Waals interaction.[3] A $2\times2\times1$ *k*-point grid is used for the (diammonium)$(FA)_{n-1}Sn_nX_{3n+1}$ (n = 1 - 4), which is good enough based on our test computation. The electronic structures and the optical properties (with $4\times4\times1$ *k*-point grid) are computed by using the PBE0 functional with a cutoff energy of 400 eV.[4] The selection of the PBE0 functional is based on a previous benchmark test for 2D tin halide perovskite ((4AMP)$(FA)_{n-1}Sn_nI_{3n+1}$ system, where 4AMP refers to 4-(aminomethyl)piperidinium and n = 1, 2). In that test, the computed bandgaps based on the PBE0 functional are in good agreement with measured bandgaps.[5] The optical absorption coefficient is given by $\frac{\sqrt{2}e}{\hbar c}\left[\left({\varepsilon_1}^2+{\varepsilon_2}^2\right)^{\frac{1}{2}}-\varepsilon_1\right]^{\frac{1}{2}}$, where ε_1 and ε_2 are real and imaginary part of dielectric function, respectively.

For the diammoniums and all organic molecules considered, their neutral and charged geometries are optimized by using the PBE0 hybrid functional and the 6-31G** basis set, as implemented in Gaussian 09 code. The optical absorption spectra are computed by using the time-dependent DFT method. The rates of charge transfer between neighboring diammoniums and molecules are described by the Marcus theory[6] following the equation $k_{h/e}=\frac{4\pi^2}{h}\frac{1}{\sqrt{4\pi\lambda_{h/e}k_BT}}{V_{h/e}}^2 exp(-\frac{\lambda_{h/e}}{4k_BT})$, where T is temperature, k_B is Boltzmann constant, h is Plank constant, and $\lambda_{h/e}$ is the hole or electron reorganization energy. The latter is the energy cost of charging a single molecule within the crystal; $V_{h/e}$ refers to the electronic coupling which reflects to strength of the interaction in dimer configuration, and is calculated by using the Q-Chem code.[7] The formula used for this calculation is $V_{AB}=\frac{|H_{AB}-S_{AB}(H_{AA}+H_{BB})/2|}{1-S_{AB}^2}$, with $H_{AB}=\langle\psi_A|H|\psi_B\rangle$ and $S_{AB}=\langle\psi_A|\psi_B\rangle$.[8] These calculations are performed at the unrestricted Hartree-Fock level with 6-31G** basis set. The hole or electron motility is estimated by using the Einstein relation $\mu=\frac{eD}{k_BT}$, where e is the electron charge and D is the charge diffusion coefficient which can be evaluated from $D=\frac{1}{2n}\sum_i d_i^2k_iP_i$, where n is the spatial dimension, k_i is the charge transfer rate along each direction, d_i is the corresponding hopping distance (defined by the distance between the centroids of two molecules) and P_i is relative probability given by $P_i=\frac{k_i}{\sum_i k_i}$.

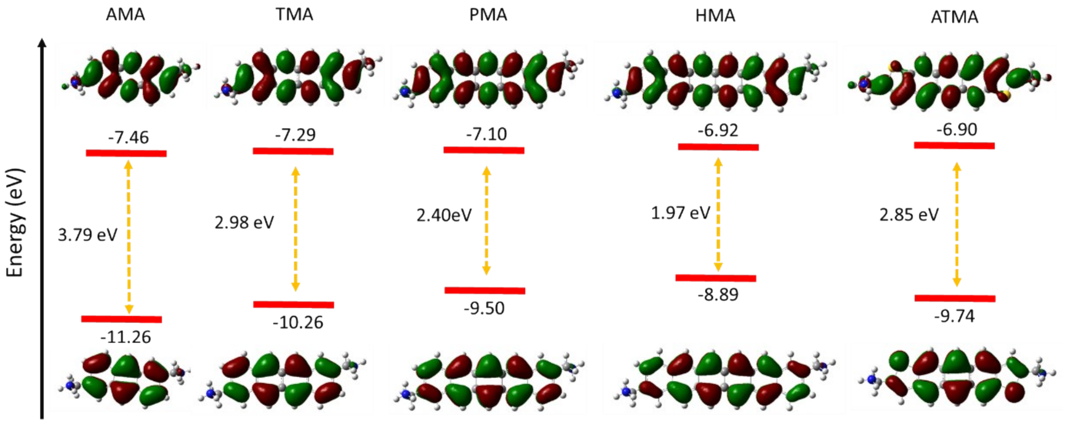

Figure S1. Computed frontier orbitals of diammouniums, AMA, TMA, PMA, HMA and ATMA based on the PBE0 functional.

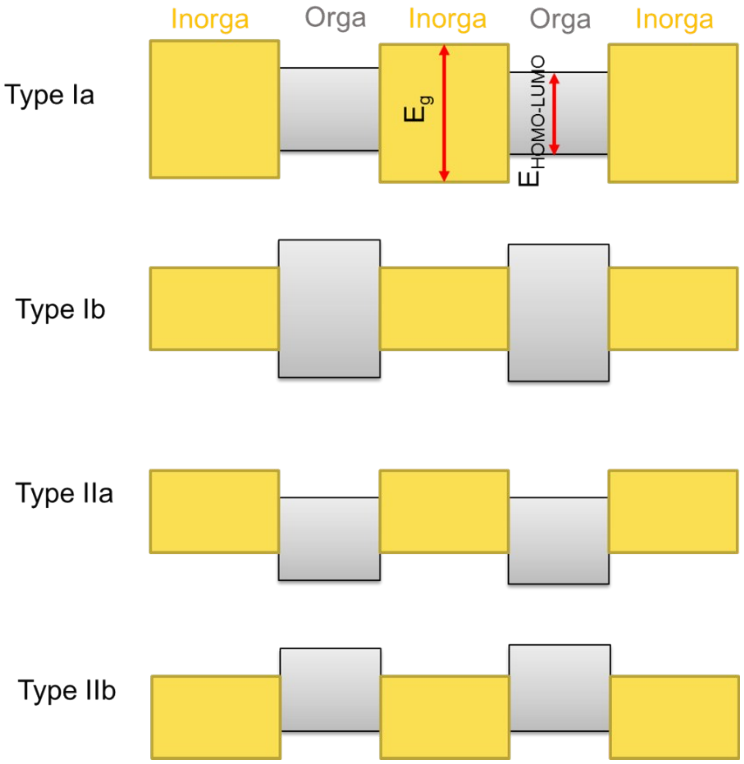

Figure S2. Possible four band alignments (type Ia, type Ib, type IIa and type IIb) for alternating 2D OIHPs with the bandgap of organic and inorganic components indicated by arrows.

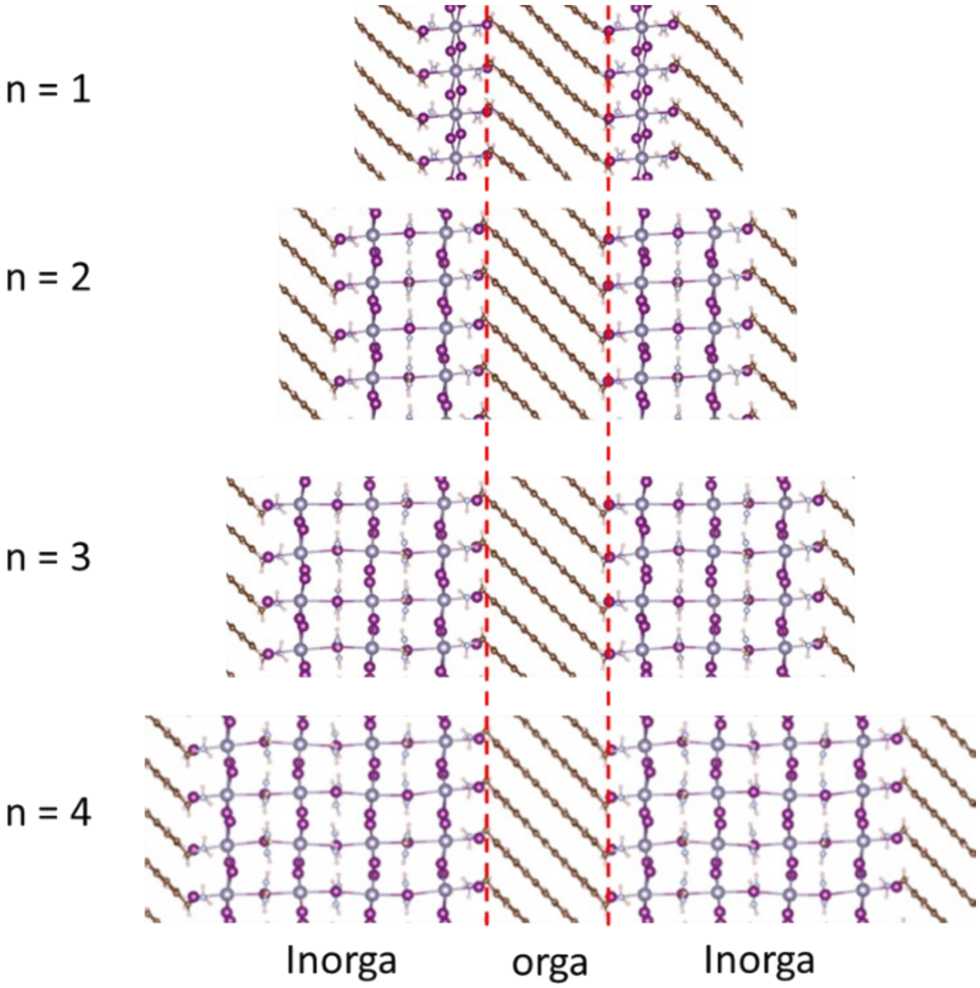

Figure S3. Crystalline structures of 2D OIHPs (diammonium)$(FA)_{n-1}Sn_nX_{3n+1}$ (n = 1 - 4).

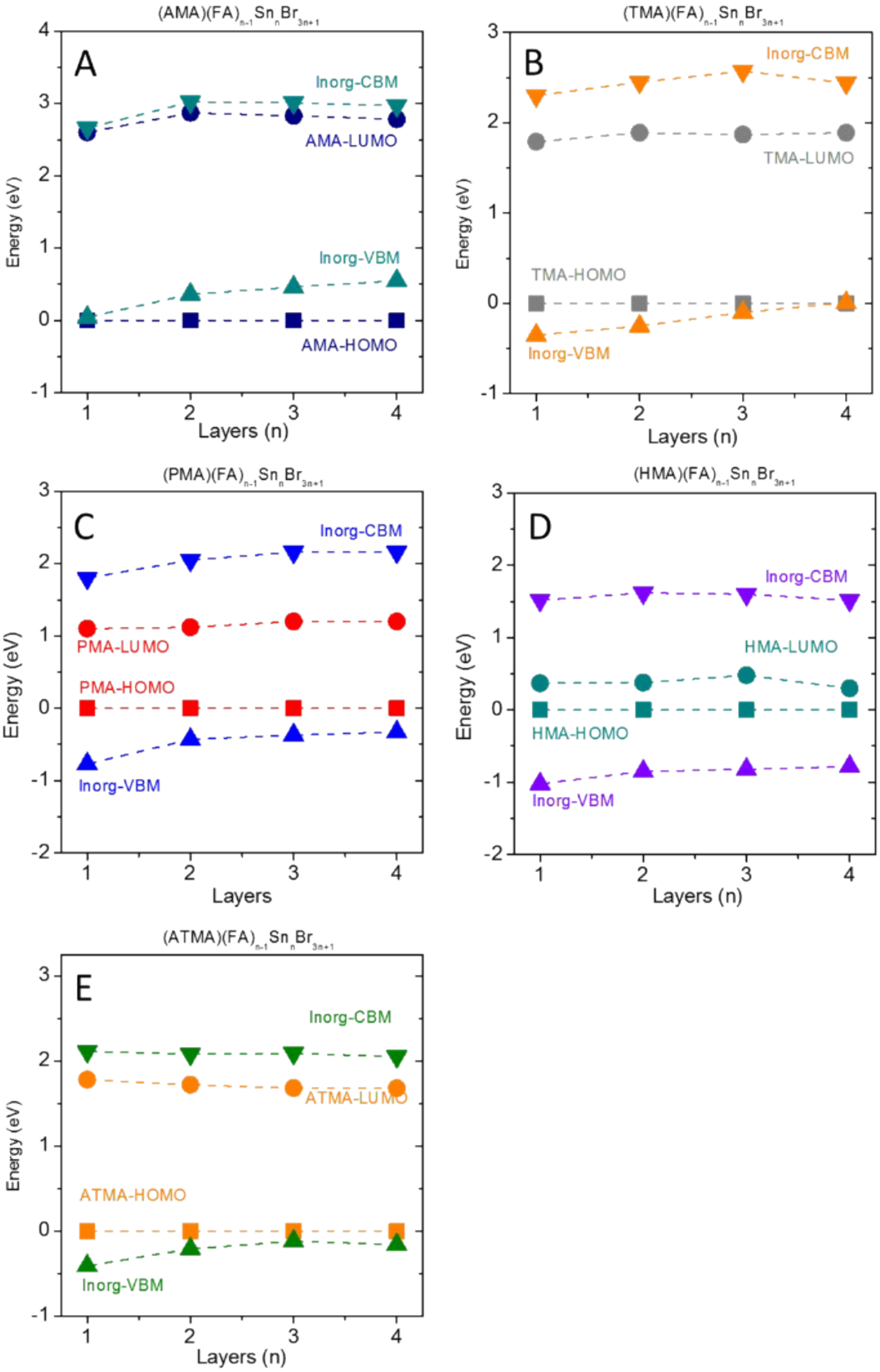

Figure S4. Computed frontier energy level of "organic" and "inorganic" components of (diammonium)(FA)$_{n-1}$Sn$_n$Br$_{3n+1}$ (n = 1 - 4), diammounium = AMA (A), TMA (B), PMA (C), HMA (D) and ATMA (E), based on the PBE0 functional. The HOMO of "organic" components are the reference energy.

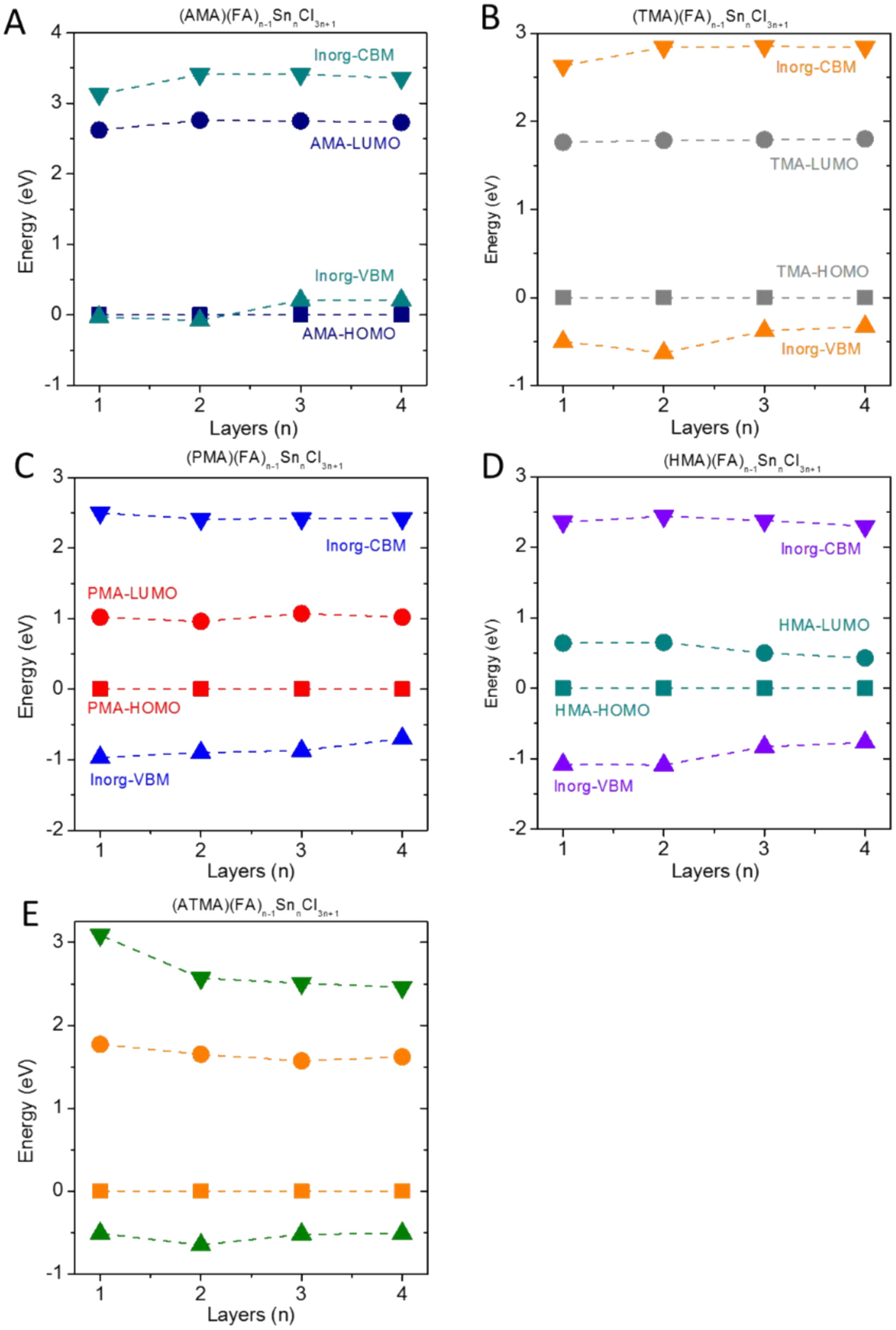

Figure S5. Computed frontier energy level of “organic” and “inorganic” components of (diammonium)$(FA)_{n-1}Sn_nCl_{3n+1}$ (n = 1 - 4), diammounium = AMA (A), TMA (B), PMA (C), HMA (D) and ATMA (E), based on the PBE0 functional. The HOMO of “organic” components are the reference energy.

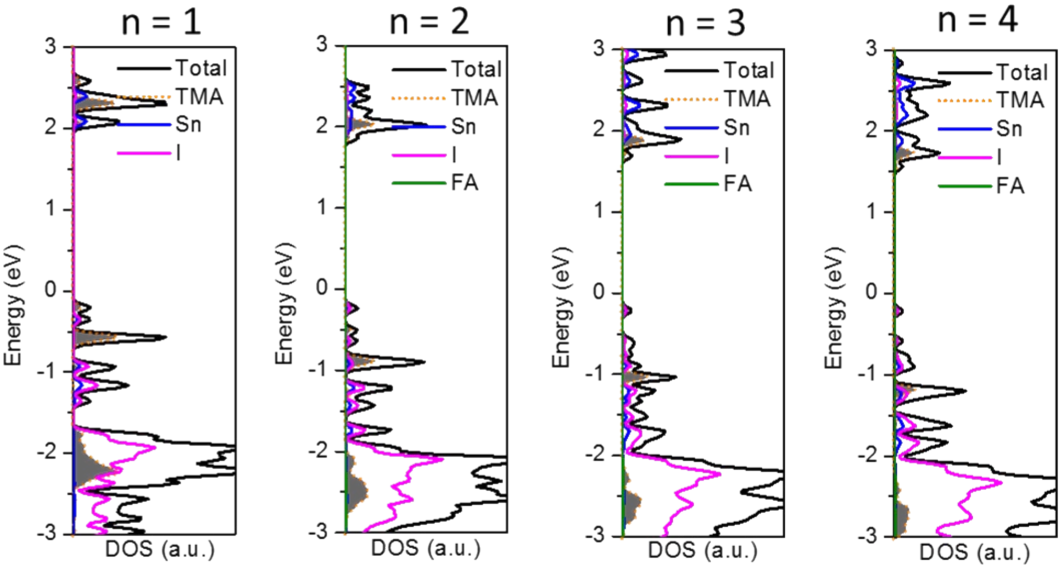

Figure S6. Computed TDOSs and PDOSs of $(TMA)(FA)_{n-1}Sn_nI_{3n+1}$ (n = 1 - 4) based on the PBE0 functional.

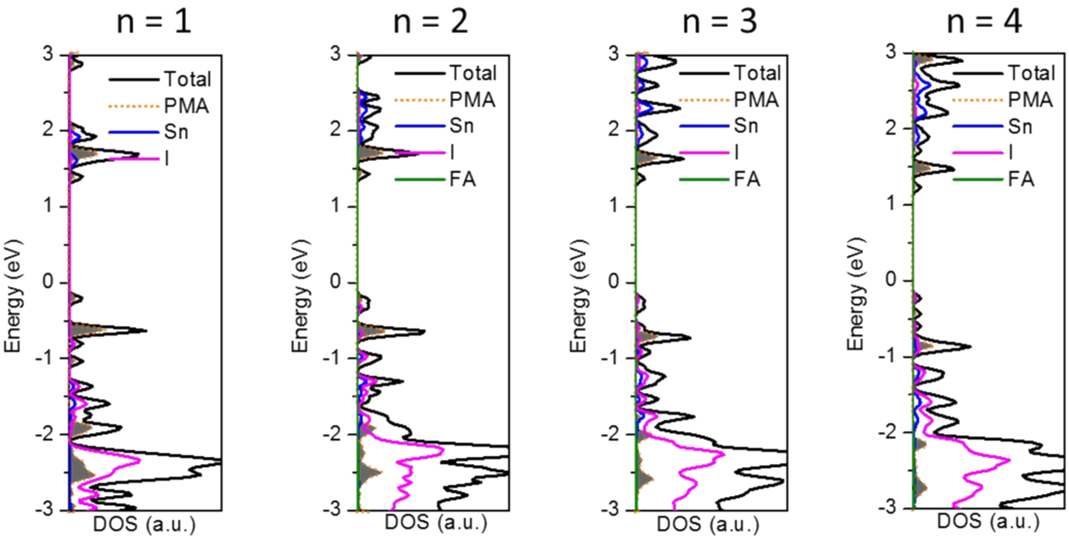

Figure S7. Computed TDOSs and PDOSs of $(PMA)(FA)_{n-1}Sn_nI_{3n+1}$ (n = 1 - 4) based on the PBE0 functional.

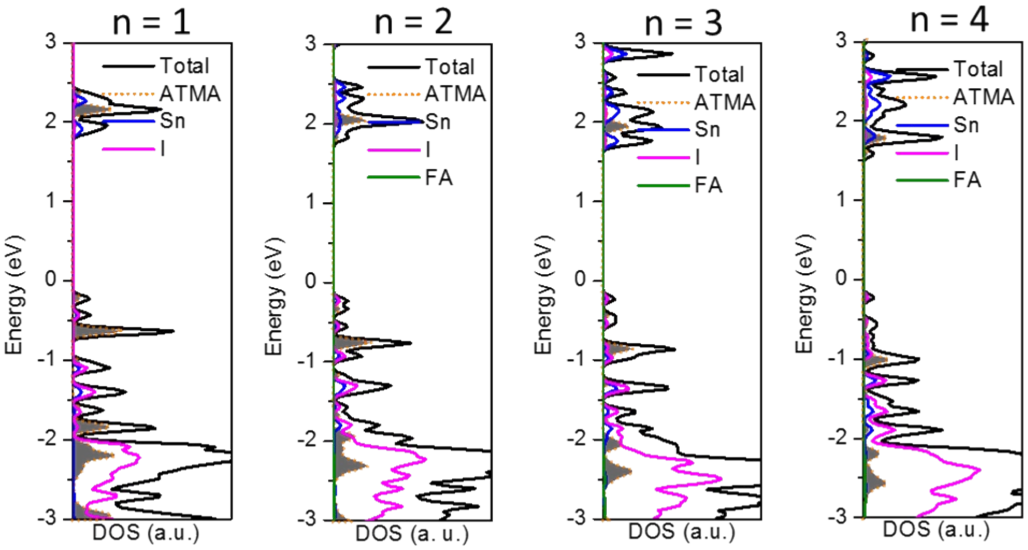

Figure S8. Computed TDOSs and PDOSs of $(ATMA)(FA)_{n-1}Sn_nI_{3n+1}$ (n = 1 - 4) based on the PBE0 functional.

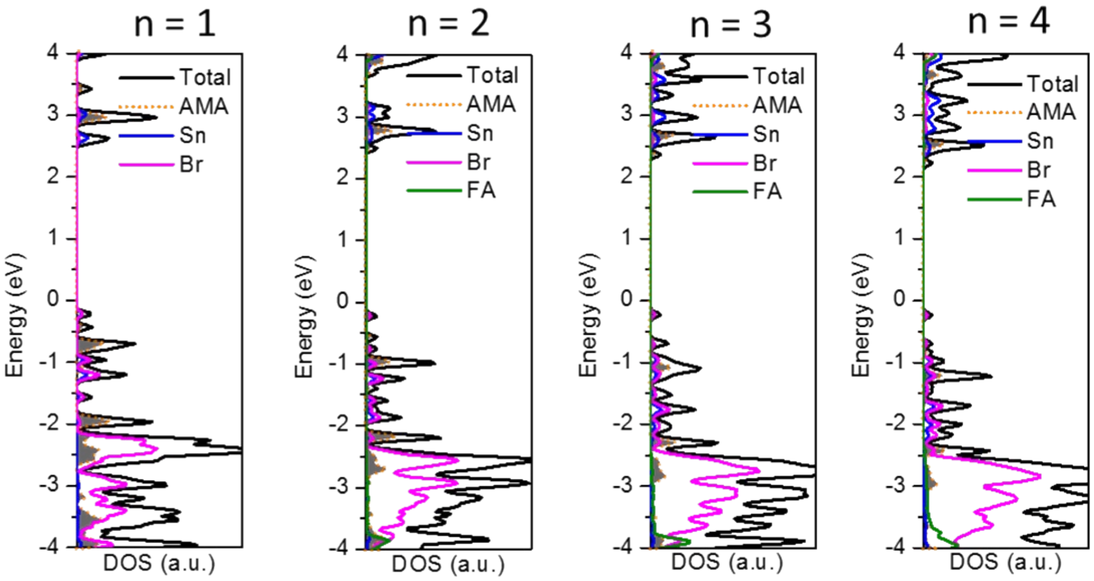

Figure S9. Computed TDOSs and PDOSs of $(AMA)(FA)_{n-1}Sn_nBr_{3n+1}$ (n = 1 - 4) based on the PBE0 functional.

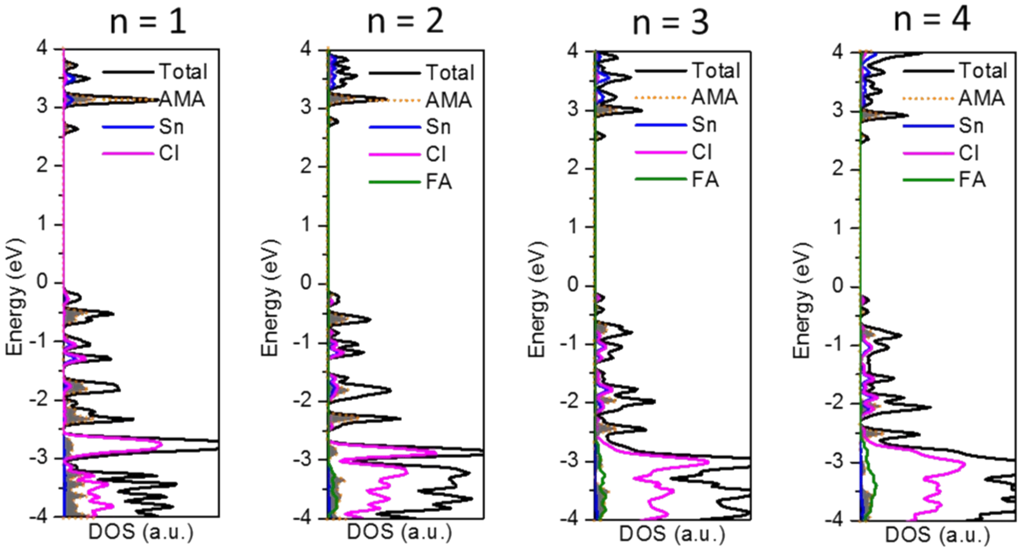

Figure S10. Computed TDOSs and PDOSs of $(AMA)(FA)_{n-1}Sn_nCl_{3n+1}$ (n = 1 - 4) based on the PBE0 functional.

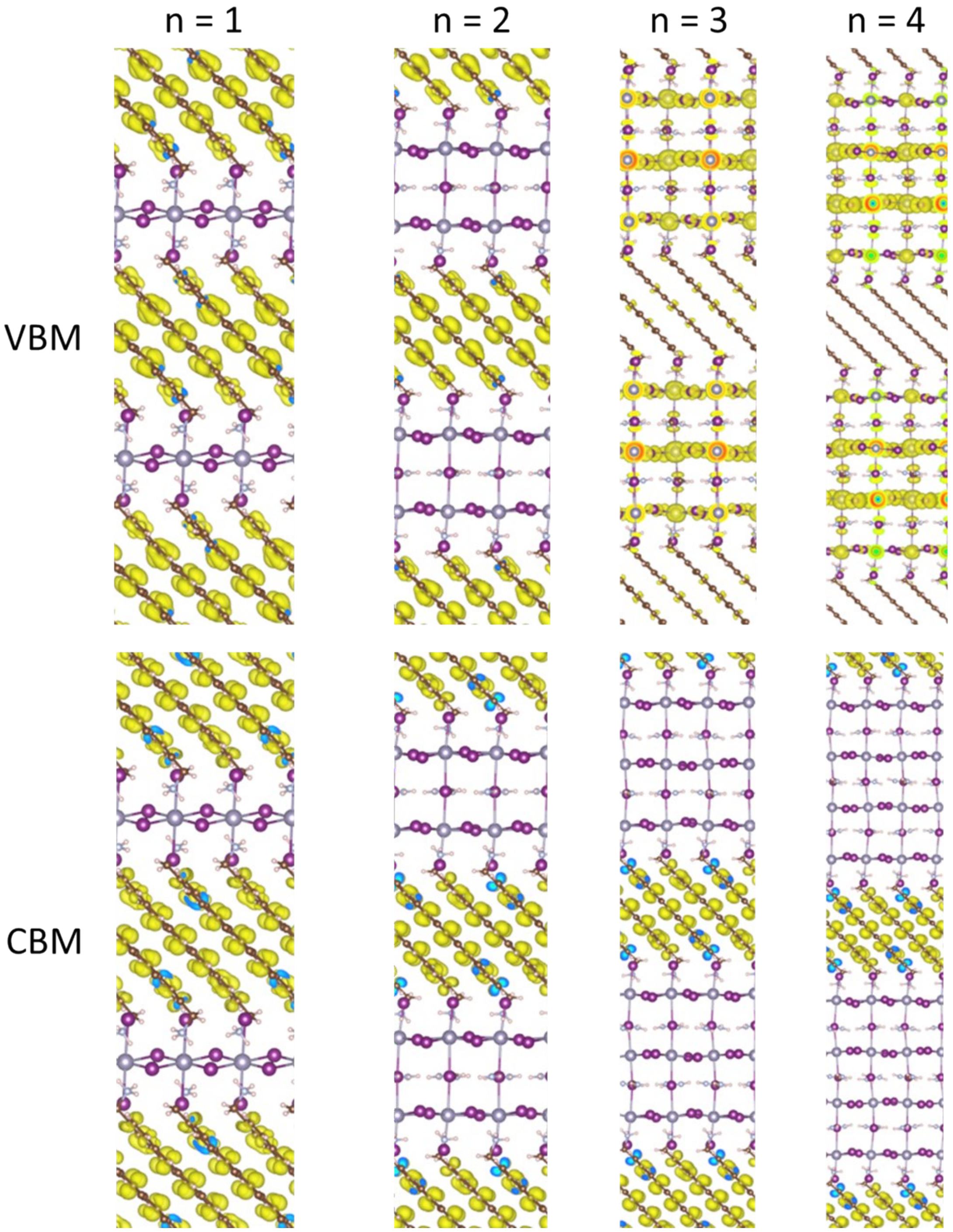

Figure S11. Computed charge density distribution of the highest VB and lowest CB of a periodic slab model of (PMA)$(FA)_{n-1}Sn_nI_{3n+1}$ (n = 1 - 4) based on the PBE0 functional.

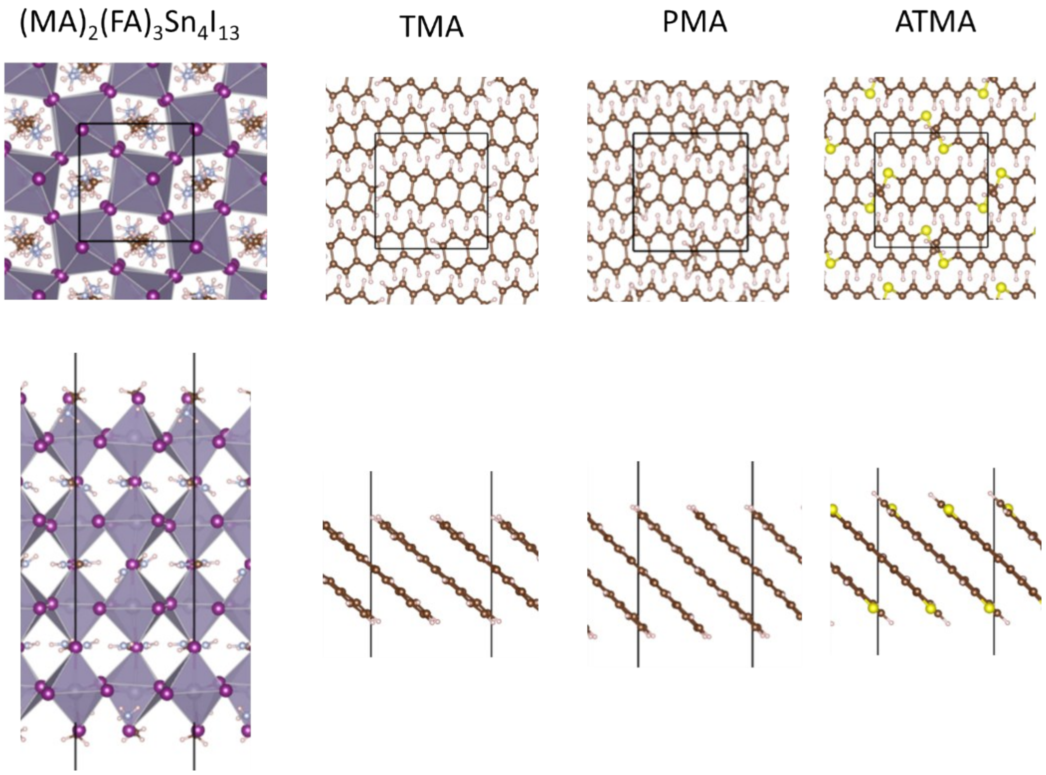

Figure S12. Crystalline structures of 2D $(MA)_2(FA)_3Sn_4I_{13}$, 2D tetracenes, 2D pentacenes and 2D anthra[2,3-*b*:7,8-*b*′]dithiophene, viewed from top (top) and side (bottom). The crystal structures of the 2D materials are obtained by shearing the corresponding $-CH_2NH_3$ group of the “organic” components in the corresponding 2D OIHPs. Then the “organic component” and “inorganic component” are saturated by H and separated.

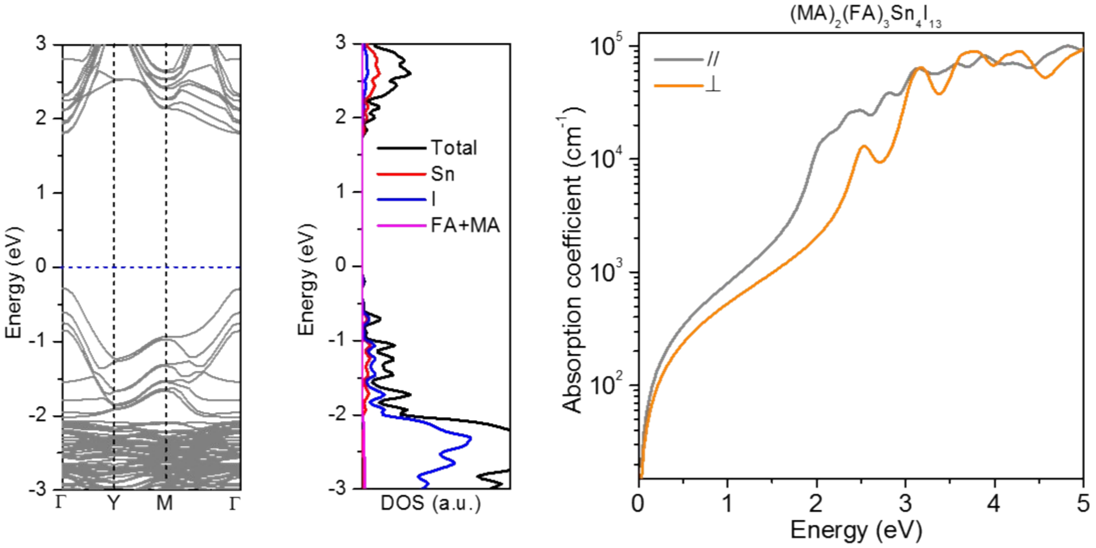

Figure S13. Computed band structures, DOSs and optical absorption spectrum of $(MA)_2(FA)_3Sn_4I_{13}$ based on the PBE0 functional. (//: parallel to xy; ⊥: perpendicular to xy).

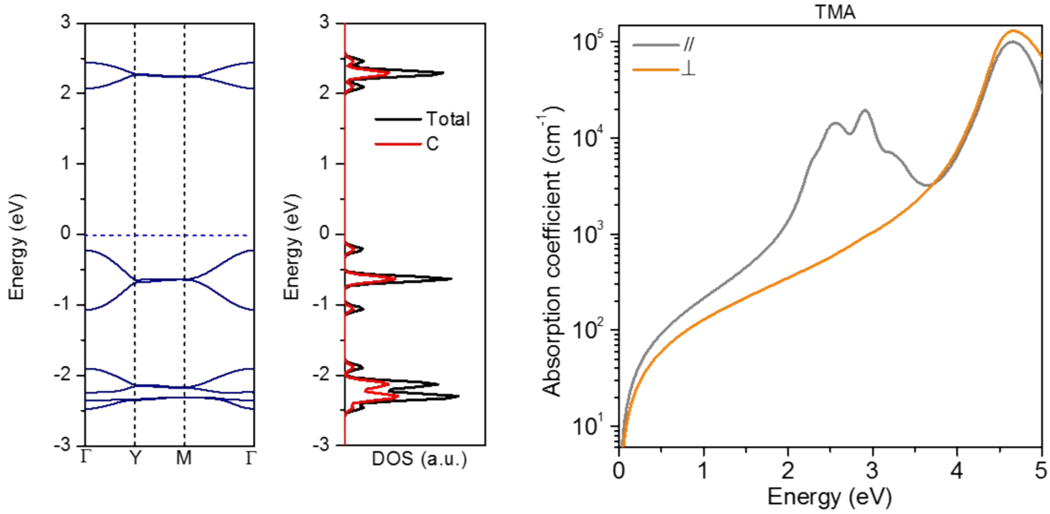

Figure S14. Computed band structures, DOSs and optical absorption spectrum of 2D tetracenes based on the PBE0 functional. (//: parallel to xy; ⊥: perpendicular to xy).

.

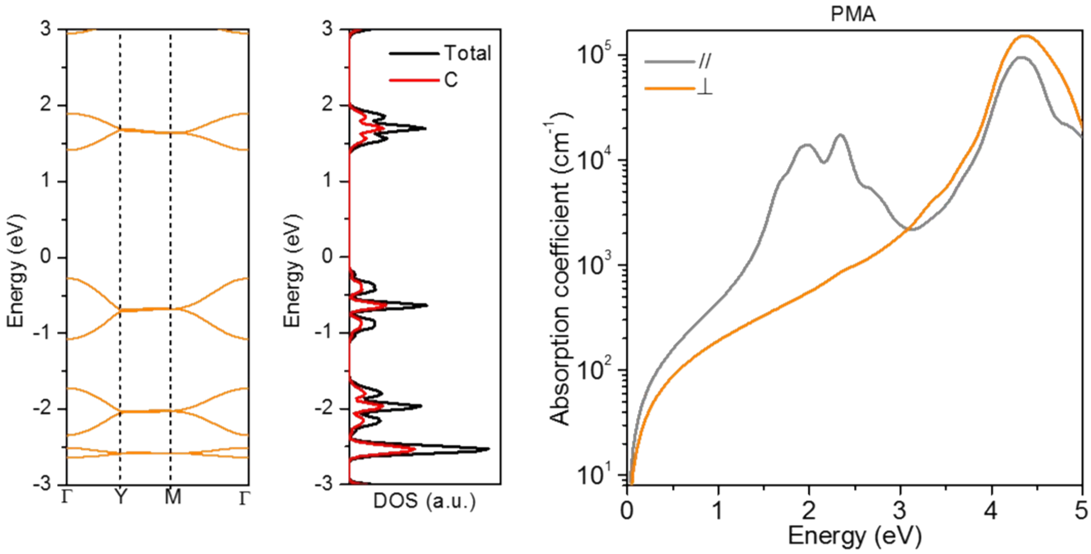

Figure S15. Computed band structures, DOSs and optical absorption spectrum of 2D pentacenes based on the PBE0 functional. (//: parallel to xy; ⊥: perpendicular to xy).

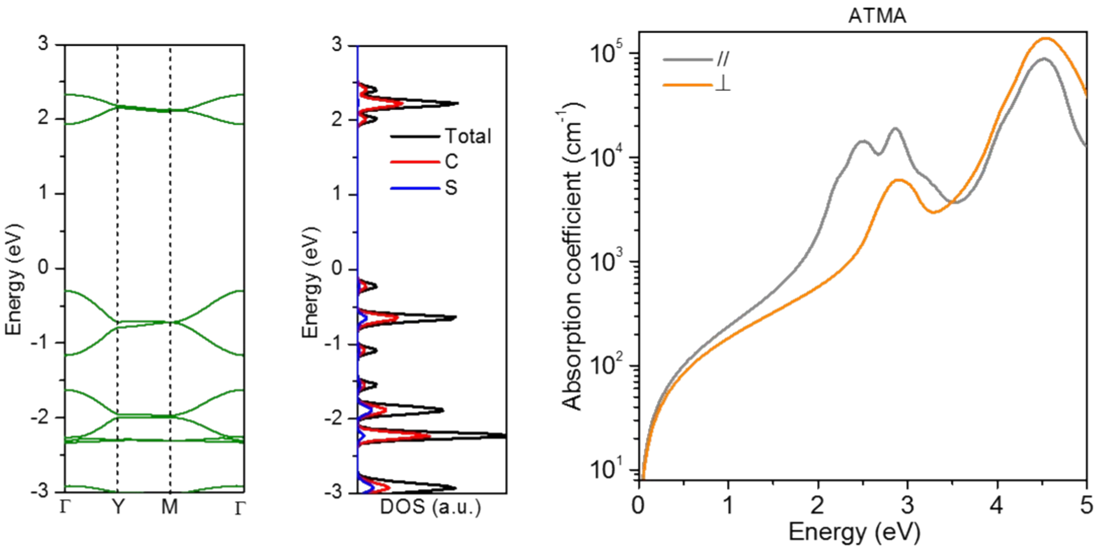

Figure S16. Computed band structures, DOSs and optical absorption spectrum of 2D anthra[2,3-*b*:7,8-*b′*]dithiophene based on the PBE0 functional. (//: parallel to xy; ⊥: perpendicular to xy).

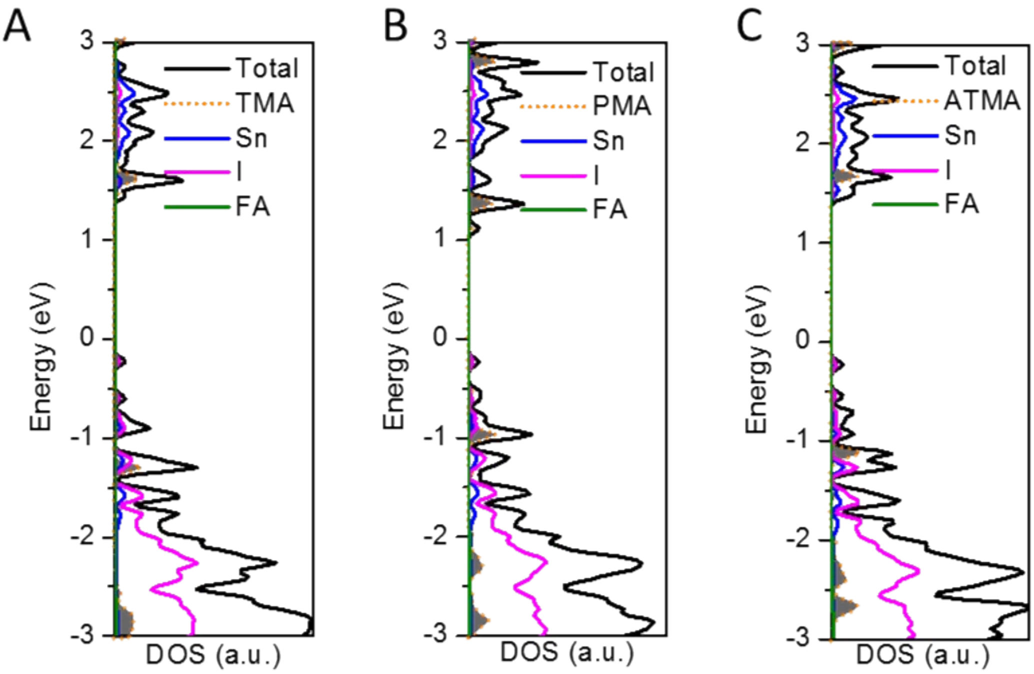

Figure S17. Computed TDOSs and PDOSs of (TMA)(FA)$_3$Sn$_4$I$_{13}$ (A), (PMA)(FA)$_3$Sn$_4$I$_{13}$ (B) and (ATMA)(FA)$_3$Sn$_4$I$_{13}$ (C) based on the PBE0 functional with consideration of SOC effect.

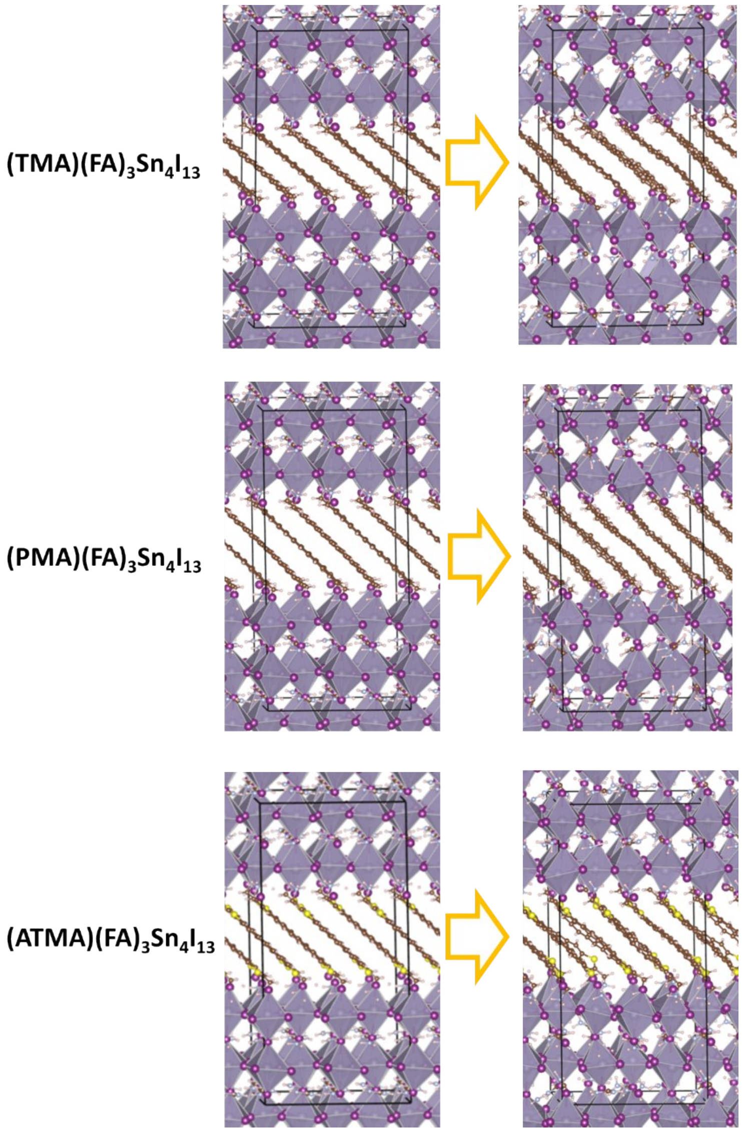

Figure S18. Snapshots of (TMA)(FA)$_3$Sn$_4$I$_{13}$, (PMA)(FA)$_3$Sn$_4$I$_{13}$ and (ATMA)(FA)$_3$Sn$_4$I$_{13}$ at initial (left) and ending 5 ps (right) of the AIMD simulation with temperature being controlled at 300 K (in *NVT* ensemble).

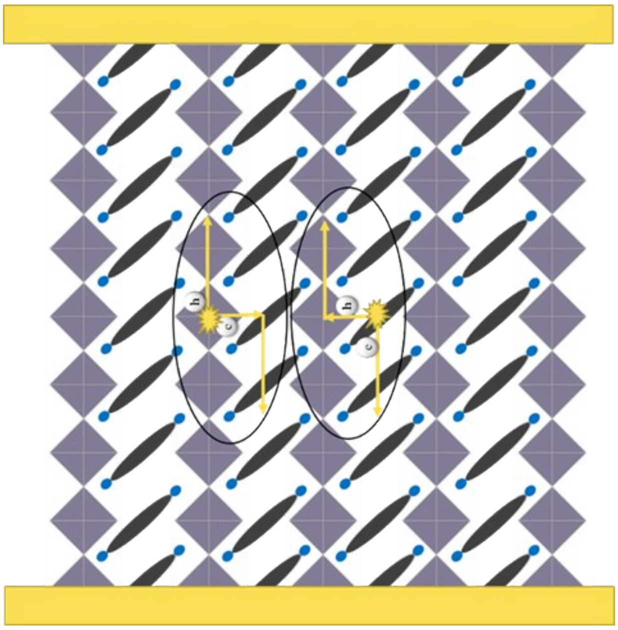

Figure S19. Schematic representation of the 2D DJ OIHPs orientation with respect to the substrate.

TABLE S1. Calculated reorganization energies (eV) of PMA, TMA and ATMA.

	PMA	TMA	ATMA
electron	0.22	0.28	0.36
hole	0.17	0.21	0.19

TABLE S2. Calculated charge transfer parameters and mobility of the PMA.

	channel	$V_{h/e}$ (meV)	d (Å)	k_i (s^{-1})	D (cm^2/s)	μ ($cm^2V^{-1}s^{-1}$)
electron	1	-110.4	6.32	5.34×10^{13}	5.34×10^{-2}	2.06
	2	-0.0026	9.08	2.95×10^{6}		
hole	1	-147.85	6.32	1.63×10^{14}	1.62×10^{-1}	6.25
	2	0.0025	9.08	4.61×10^{6}		

TABLE S3. Calculated charge transfer parameters and mobility of the TMA.

	channel	$V_{h/e}$ (meV)	d (Å)	k_i (s^{-1})	D (cm^2/s)	μ ($cm^2V^{-1}s^{-1}$)
electron	1	77.2	6.27	1.33×10^{13}	1.31×10^{-2}	0.51
	2	0.0031	9.08	1.58×10^{6}		
hole	1	168.7	6.27	1.38×10^{14}	1.35×10^{-1}	5.24
	2	0.0019	9.08	1.68×10^{6}		

TABLE S4. Calculated charge transfer parameters and mobility of the ATMA.

	channel	$V_{h/e}$ (meV)	d (Å)	k_i (s^{-1})	D (cm^2/s)	μ ($cm^2V^{-1}s^{-1}$)
electron	1	-81.96	6.30	5.91×10^{12}	5.86×10^{-3}	0.23
	2	-0.0075	8.90	5.01×10^{6}		
hole	1	-151.5	6.30	1.41×10^{14}	1.40×10^{-1}	5.42
	2	0.005	8.90	1.51×10^{7}		

TABLE S5. Calculated reorganization energies (eV) of tetracene, pentacene and anthra[2,3-*b*:7,8-*b*′]dithiophene.

	pentacene	tetracene	anthra[2,3-*b*:7,8-*b*′]dithiophene
electron	0.12	0.17	0.17
hole	0.10	0.12	0.10

TABLE S6. Calculated charge transfer parameters and mobility of the pentacene.

	channel	$V_{h/e}$ (meV)	d (Å)	k_i (s^{-1})	D (cm^2/s)	μ ($cm^2V^{-1}s^{-1}$)
electron	1	98.5	6.28	1.48×10^{14}	1.46×10^{-1}	5.65
	2	-0.0034	9.04	1.80×10^{7}		
hole	1	176.9	6.28	6.22×10^{14}	6.13×10^{-1}	23.7
	2	0.0031	9.04	1.91×10^{7}		

TABLE S7. Calculated charge transfer parameters and mobility of the tetracene.

	channel	$V_{h/e}$ (meV)	d (Å)	k_i (s^{-1})	D (cm^2/s)	μ ($cm^2V^{-1}s^{-1}$)
electron	1	64.9	6.31	3.44×10^{13}	3.42×10^{-2}	1.32
	2	0.002	9.05	3.26×10^{6}		
hole	1	-181.2	6.31	5.00×10^{14}	4.97×10^{-1}	19.2
	2	0.0024	9.05	8.81×10^{6}		

TABLE S8. Calculated charge transfer parameters and mobility of the anthra[2,3-*b*:7,8-*b'*]dithiophene.

	channel	$V_{h/e}$ (meV)	d (Å)	k_i (s^{-1})	D (cm^2/s)	μ ($cm^2V^{-1}s^{-1}$)
electron	1	95.4	6.21	7.40×10^{13}	7.14×10^{-2}	2.76
	2	-0.0077	8.89	4.83×10^{7}		
hole	1	-194.7	6.21	7.48×10^{14}	7.22×10^{-1}	27.9
	2	0.0068	8.89	9.09×10^{7}		

Supplementary Reference

[1] G. Kresse, J. Furthmüller, *Comput. Mater. Sci.* **1996**, *6*, 15.

[2] G. Kresse, D. Joubert, *Phys. Rev. B* **1999**, *59*, 1758.

[3] S. Grimme, J. Antony, S. Ehrlich, H. Krieg, *J. Chem. Phys.* **2010**, *132*, 154104.

[4] J. Paier, R. Hirschl, M. Marsman, G. Kresse, *J. Chem. Phys.* **2005**, *122*, 234102

[5] M. Chen, M.-G. Ju, M. Hu, Z. Dai, Y. Hu, Y. Rong, H. Han, X. C. Zeng, Y. Zhou, N. P. Padture, *ACS Energy Lett.* **2019**, *4*, 276.

[6] R. A. Marcus, *Rev. Mod. Phys.* **1993**, *65*, 599.

[7] Y. Shao, L. F. Molnar, Y. Jung, J. Kussmann, C. Ochsenfeld, S. T. Brown, A. T. B. Gilbert, L. V. Slipchenko, S. V. Levchenko, D. P. O'Neill, *Phys. Chem. Chem. Phys.* **2006**, *8*, 3172.

[8] A. Farazdel, M. Dupuis, E. Clementi, A. Aviram, *J. Am. Chem. Soc.* **1990**, *112*, 4206.